nature portfolio

https://doi.org/10.1038/s41586-024-07362-8

Supplementary information

Chemical short-range disorder in lithium oxide cathodes

In the format provided by the authors and unedited

Supplementary information

Chemical short-range disorder in lithium oxide cathodes

Qidi Wang[1], Zhenpeng Yao[2], Jianlin Wang[3], Hao Guo[4], Chao Li[5], Dong Zhou[6], Xuedong Bai[3], Hong Li[7], Baohua Li[8], Marnix Wagemaker[1], Chenglong Zhao[1]

[1]Department of Radiation Science and Technology, Delft University of Technology, Delft, 2629JB, the Netherlands.

[2]The State Key Laboratory of Metal Matrix Composites, Center of Hydrogen Science, School of Materials Science and Engineering, Shanghai Jiao Tong University, Shanghai, 200240, China.

[3]State Key Laboratory for Surface Physics, Institute of Physics, Chinese Academy of Sciences, Beijing, 100190, China.

[4]Neutron Scattering Laboratory, Department of Nuclear Physics, China Institute of Atomic Energy, Beijing, 102413, China.

[5]Shanghai Key Laboratory of Magnetic Resonance, School of Physics and Electronic Science, East China Normal University, Shanghai, 200062, China.

[6]Helmholtz-Zentrum Berlin für Materialien und Energie, Berlin, 14109, Germany.

[7]Key Laboratory for Renewable Energy, Institute of Physics, Chinese Academy of Sciences, Beijing, 100190, China.

[8]Shenzhen Key Laboratory on Power Battery Safety and Shenzhen Geim Graphene Center, School of Shenzhen International Graduate, Tsinghua University, Guangdong 518055, China.

Table of Contents

Supplementary Notes

Supplementary Note 1

Structure transformations among the layered, disordered, and spinel structures.

The ordered layered structure is characterized by alternating MeO_2 and LiO_2 slabs, resulting in a ratio of $d_{(O–Li–O)}/d_{(O–Me–O)}$ above 1, which is due to the stronger Me−O interaction compared to the Li−O interaction, making the perpendicular distance between the two oxygen sheets enclosing the Me ions of $d_{(O–Me–O)}$ smaller than $d_{(O–Li–O)}$[1]. The structural transition from the layered to disordered structure requires half of the Me ions to migrate into the LiO_2 slabs, which leads to completely disordered MeO_2 and LiO_2 slabs, resulting in the ratio of $d_{(O–Li–O)}/d_{(O–Me–O)}$ to become unity. The structural transition from layered to spinel structure requires about 1/4 of the Me ions to migrate into LiO_2 slabs, resulting in a $d_{(O–Li–O)}/d_{(O–Me–O)}$ ratio that equals 1 for the $LiMeO_2$ and approaches 1 for the $Li_{0.5}MeO_2$, respectively.

Supplementary Note 2

Extension to $Li_xMe_yO_2$ systems

To evaluate if this CSRD approach is more generally applicable to other oxide materials, we verify its application to the multiple-principal-element $Li_xMe_yO_2$ system, where Me can be a mixture of two elements as the proof of concept. The weighted average ionic potential $\overline{\Phi_{Me}}$ of the representative $Li_{1/2}MeO_2$, $Li_{2/3}Me_{5/6}O_2$, $LiMeO_2$, and $Li_{4/3}Me_{2/3}O_2$ oxides are calculated by only considering the layered, disordered and spinel structures (Supplementary Fig. 21a and Supplementary Tables 5 and 6). It is found that the $\overline{\Phi_{Me}}$ for the spinel structure is distributed approximately from 55 to 65 nm^{-1}, mainly for the $Li_{1/2}MeO_2$ composition having a low Li-ion concentration. By comparison, the layered and disordered structures are in the range of 40 to 50 nm^{-1}. After analysis of the ionic potential of oxides in this range, $LiTi_{1/2}Mg_{1/2}O_2$ appears an interesting candidate to introduce locally disordered structures, having a $\overline{\Phi_{Me}}$ of 46.947 nm^{-1}. Advantages include that Mg^{2+} and Ti^{4+} ions are stable in air, relatively light and have a very similar ionic radius[2] of Mg^{2+}($R_{CN=6}$ = 0.72 Å) and Ti^{4+}($R_{CN=6}$ = 0.605 Å) to Li^{+}($R_{CN=6}$ = 0.76 Å), in equal ratio have an average Me^{3+} state (Me^{3+}=1/2Mg^{2+}+1/2Ti^{4+}), making this a suitable option to induce CSRD in layered $LiMeO_2$. The ionic potential difference between $Mg_{1/2}Ti_{1/2}$ and single Me^{3+} ions is calculated for the $LiMeO_2$ (Supplementary Fig. 21b), demonstrating a small difference between 3*d* TM ions in the 3+ state and $Mg_{1/2}Ti_{1/2}$, further suggesting the possibility to prepare layered oxide cathodes. $LiNi_{0.8}Co_{0.1}Mn_{0.1}O_2$ is an analog of the layered $LiCoO_2$, delivering a high specific capacity (> 200 mAh g^{-1}) and containing a small amount of Co[3,4]. The $\overline{\Phi_{Me}}$ is 49.568 nm^{-1}, close to that of $LiTi_{1/2}Mg_{1/2}O_2$, suggesting the latter can be introduced in $LiNi_{0.8}Co_{0.1}Mn_{0.1}O_2$ to induce local disorder, as studied in detail below.

A material with 2.0 % $LiTi_{1/2}Mg_{1/2}O_2$ and 98.0 % $LiNi_{0.8}Co_{0.1}Mn_{0.1}O_2$ was prepared based on the result of the above CSRD−$LiCoO_2$ with ~2.6% disorder (Supplementary Fig. 22a), which exhibits a similar diffraction pattern to the control material, both indexed in the O3-type layered structure under the same conditions. Atomic-resolution STEM−HAADF image indicates that the as-prepared $LiTi_{1/2}Mg_{1/2}O_2$−$LiNi_{0.8}Co_{0.1}Mn_{0.1}O_2$ material indeed shows local short-range cation disorder (Supplementary Fig. 22b). NPD result indicates 0.635% Mg and 0.557% Ti residing in the LiO_2 slabs, responsible for the formation of the CSRD structure (Supplementary Tables 7 and 8). The electrochemical properties of the CSRD−$LiTi_{1/2}Mg_{1/2}O_2$−$LiNi_{0.8}Co_{0.1}Mn_{0.1}O_2$ cathode were evaluated in

the voltage range of 2.8−4.5 V vs. Li^+/Li (Supplementary Figs. 22c−e). When cycled at 0.1C, both cathodes deliver a specific capacity of around 215 mAh g^{-1}, however, increasing to 0.5C, the CSRD−$LiTi_{1/2}Mg_{1/2}O_2$−$LiNi_{0.8}Co_{0.1}Mn_{0.1}O_2$ cathode show a higher capacity of around 206 mAh g^{-1} compared to 197 mAh g^{-1} for $LiNi_{0.8}Co_{0.1}Mn_{0.1}O_2$. Further cycled at 0.5C, the CSRD−$LiNi_{0.8}Co_{0.1}Mn_{0.1}O_2$ cathode shows significantly larger capacity retention of around 91% after 200 cycles compared to the 65% for the control $LiNi_{0.8}Co_{0.1}Mn_{0.1}O_2$ cathode after 100 cycles (Supplementary Fig. 22e). The result demonstrates that the introduction of CSRD structure can effectively increase the cycling stability of high-Ni layered cathodes.

Supplementary Figures

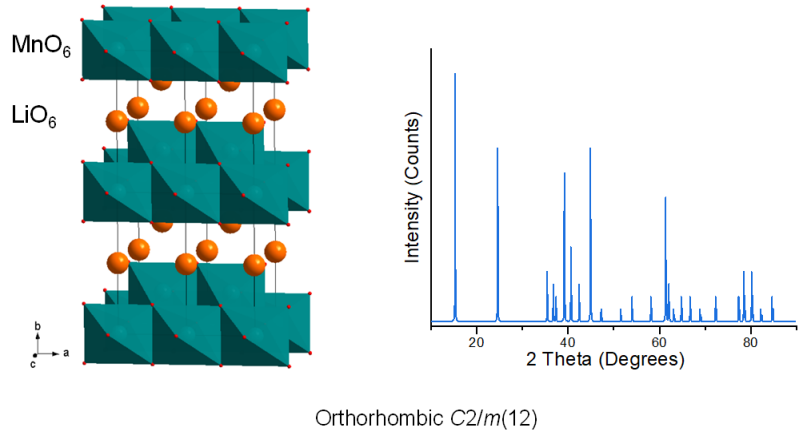

Supplementary Figure 1. Crystal structure and X-ray diffraction (XRD) pattern of orthorhombic *C*2/*m*(12) $LiMeO_2$ oxide. $LiMnO_2$ composition is selected to show the structure and diffraction information.

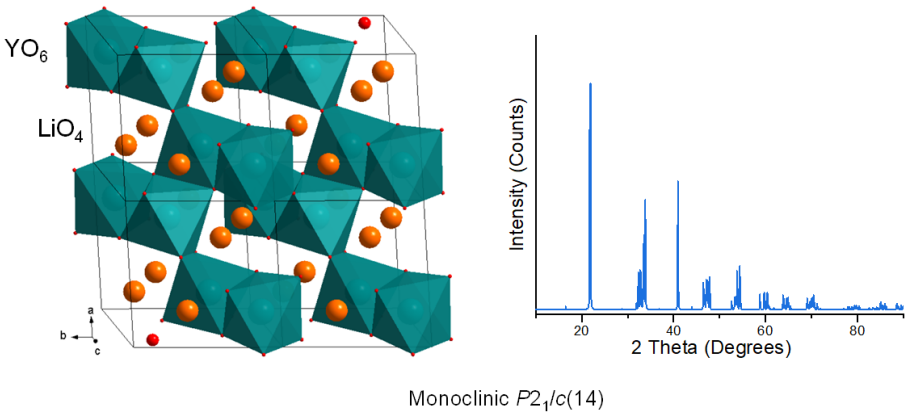

Supplementary Figure 2. Crystal structure and XRD pattern of monoclinic $P2_1/c$(14) $LiMeO_2$ oxide.

$LiYO_2$ composition is selected to show the structure and diffraction information.

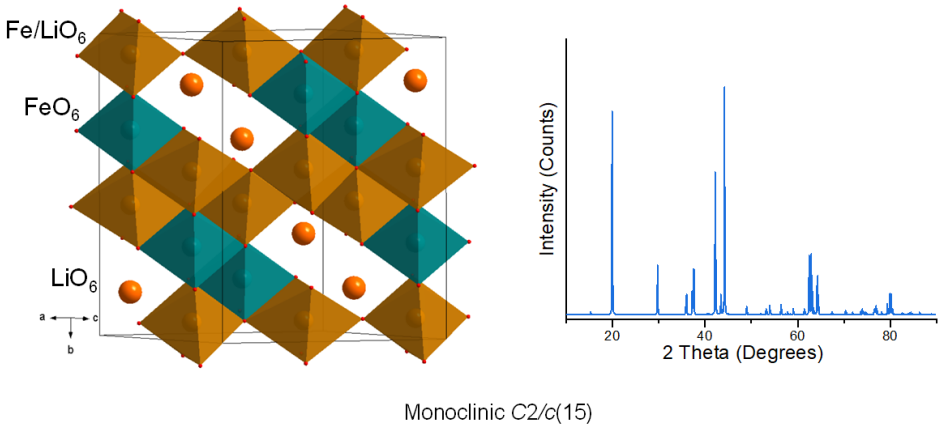

Supplementary Figure 3. Crystal structure and XRD pattern of monoclinic *C*2/*c*(15) $LiMeO_2$ oxide.

$LiFeO_2$ composition is selected to show the structure and diffraction information.

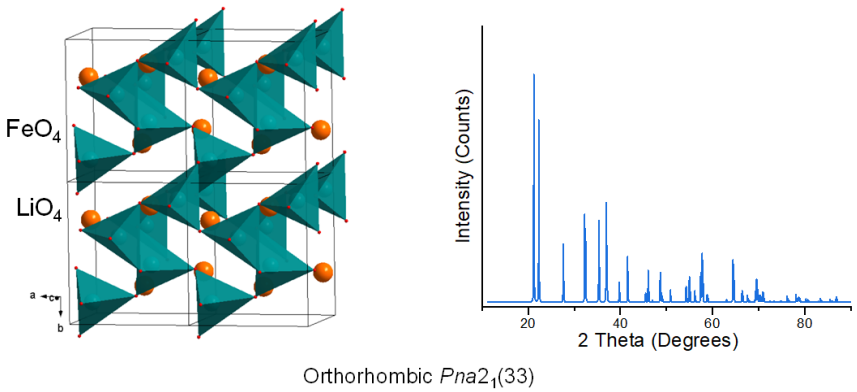

Supplementary Figure 4. Crystal structure and XRD pattern of orthorhombic *Pna*2_1(33) $LiMeO_2$ oxide. $LiFeO_2$ composition is selected to show the structure and diffraction information.

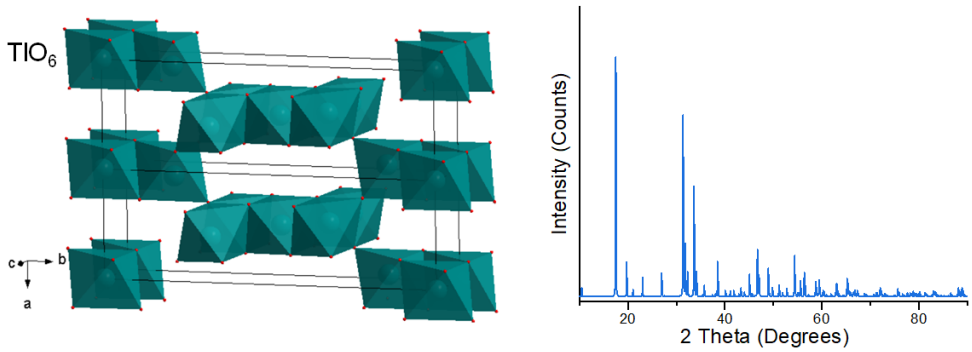

Orthorhombic *Pnnm*(58)

Supplementary Figure 5. Crystal structure and XRD pattern of orthorhombic *Pnnm*(58) $LiMeO_2$ oxide. $LiTlO_2$ composition is selected to show the structure and diffraction information.

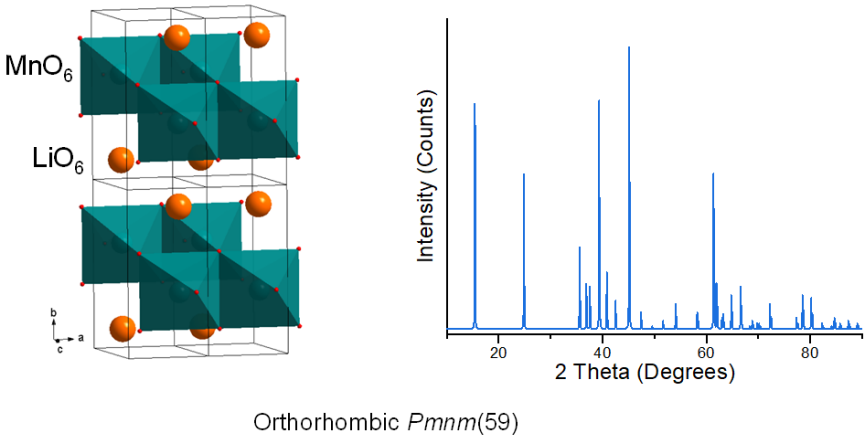

Supplementary Figure 6. Crystal structure and XRD pattern of orthorhombic *Pmnm*(59) $LiMeO_2$ oxide. $LiMnO_2$ composition is selected to show the structure and diffraction information.

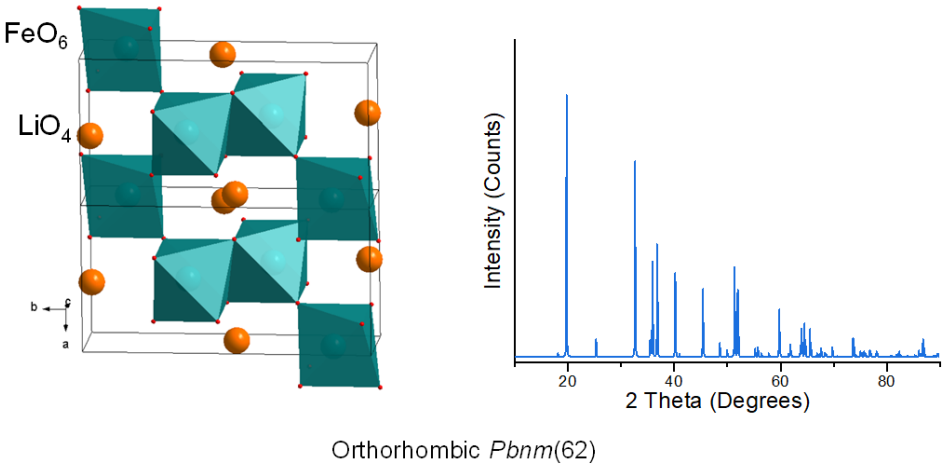

Supplementary Figure 7. Crystal structure and XRD pattern of orthorhombic *Pbnm*(62) $LiMeO_2$ oxide. $LiFeO_2$ composition is selected to show the structure and diffraction information.

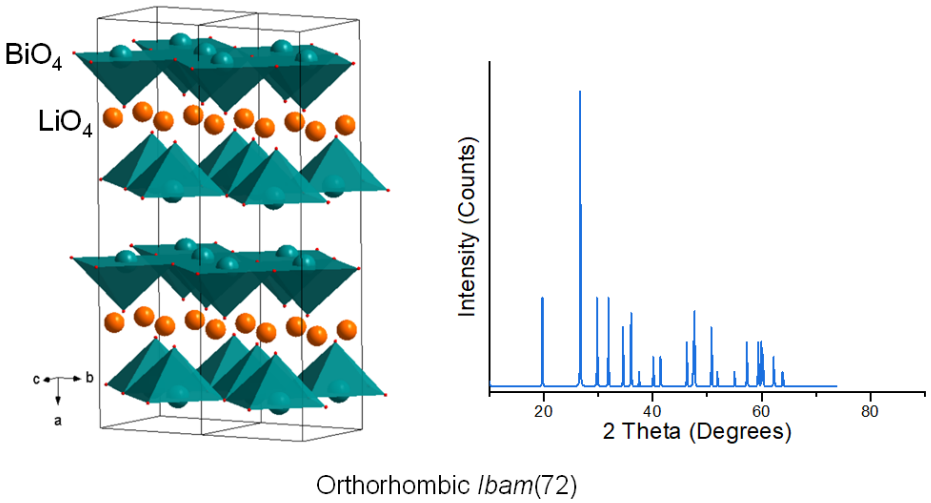

Supplementary Figure 8. Crystal structure and XRD pattern of orthorhombic *Ibam*(72) $LiMeO_2$ oxide. $LiBiO_2$ composition is selected to show the structure and diffraction information.

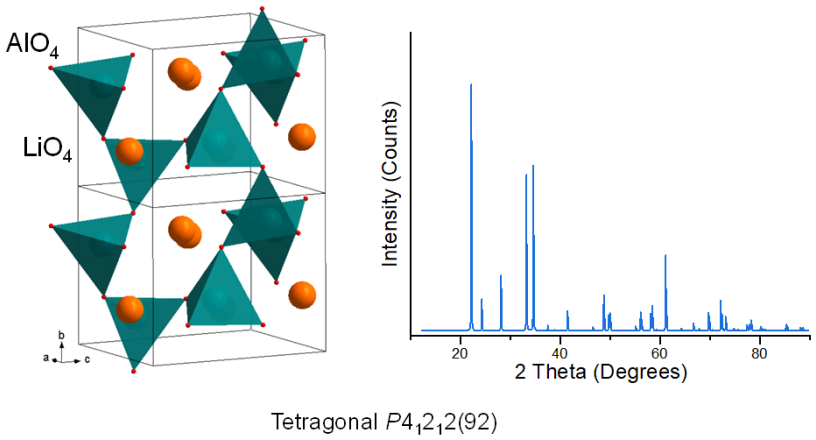

Supplementary Figure 9. Crystal structure and XRD pattern of tetragonal $P4_12_12_1(92)$ $LiMeO_2$ oxide. $LiAlO_2$ composition is selected to show the structure and diffraction information.

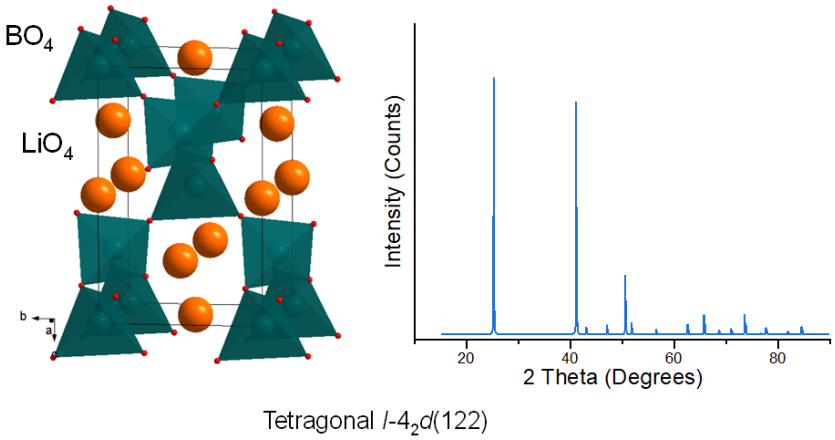

Supplementary Figure 10. Crystal structure and XRD pattern of tetragonal *I*-4$_2$*d*(122) LiMeO$_2$ oxide. LiBO$_2$ composition is selected to show the structure and diffraction information.

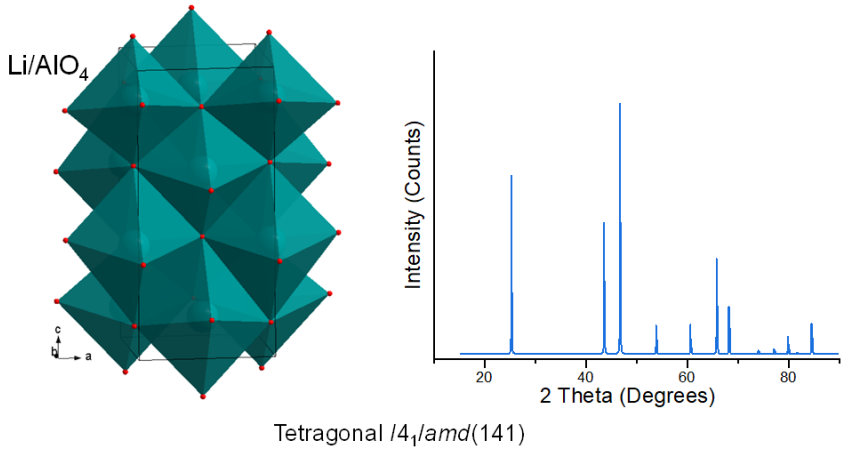

Supplementary Figure 11. Crystal structure and XRD pattern of tetragonal $I4_1/amd$(141) $LiMeO_2$ oxide. $LiAlO_2$ composition is selected to show the structure and diffraction information.

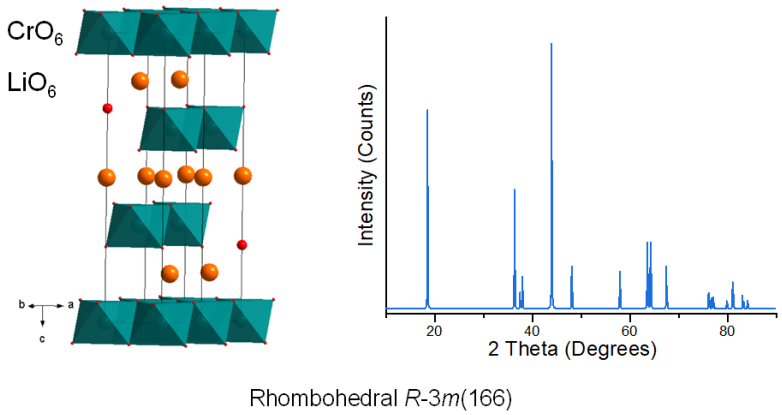

Supplementary Figure 12. Crystal structure and XRD pattern of rhombohedral *R*-3*m*(166) $LiMeO_2$ oxide. $LiCrO_2$ composition is selected to show the structure and diffraction information.

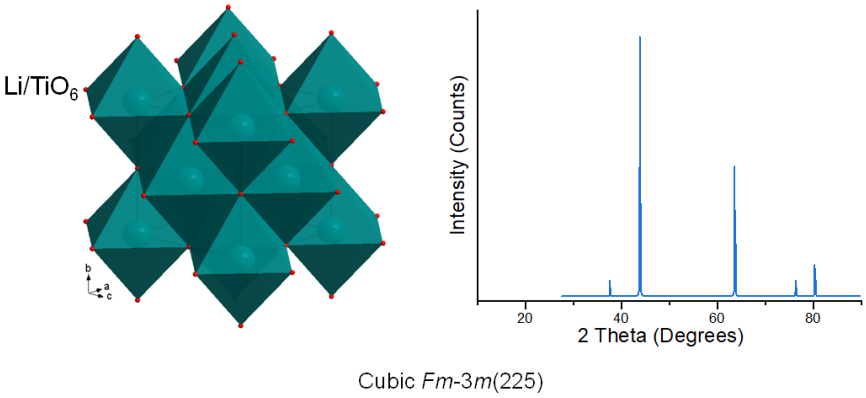

Supplementary Figure 13. Crystal structure and XRD pattern of cubic *Fm*-3*m*(225) $LiMeO_2$ oxide.

$LiTiO_2$ composition is selected to show the structure and diffraction information.

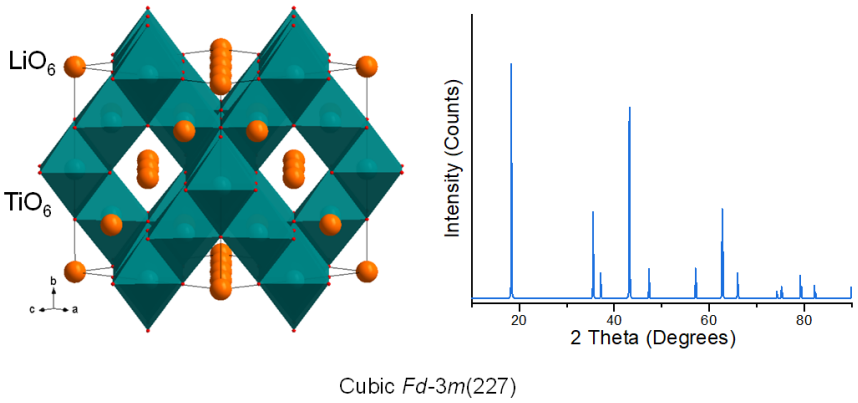

Supplementary Figure 14. Crystal structure and XRD pattern of cubic *Fd*-3*m*(227) $LiMeO_2$ oxide.

$LiTiO_2$ composition is selected to show the structure and diffraction information.

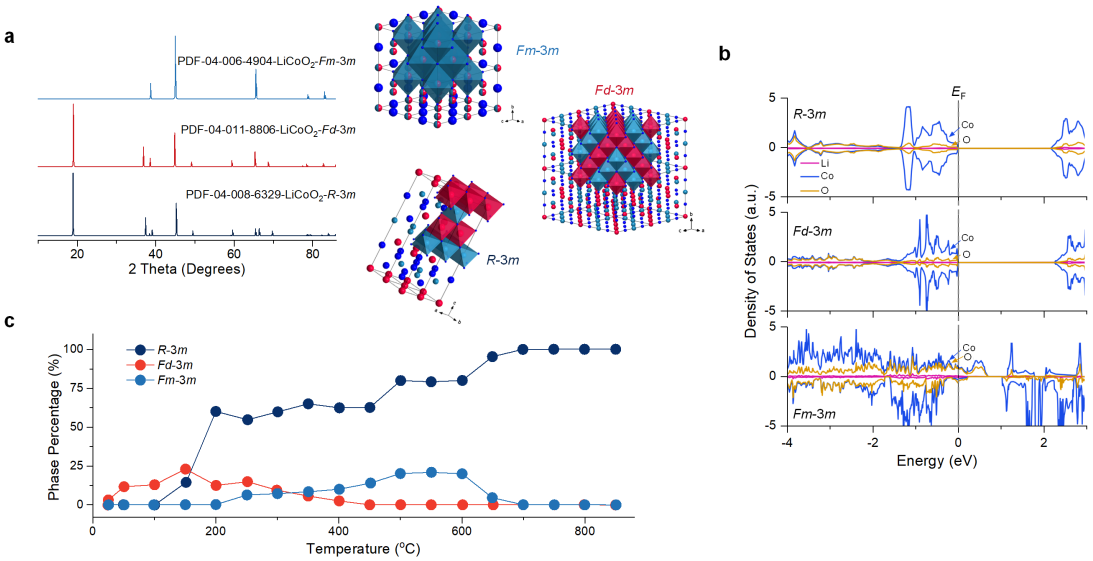

Supplementary Figure 15. Comparison of $LiCoO_2$ in different structures. a, Different structures of $LiCoO_2$ composition. **b**, PDOS of the different structures in $LiCoO_2$ composition. Fermi level is set at 0 eV. It indicates that the different structures exhibit different band gaps. **c**, Crystal structure evolution of $LiCoO_2$ composition at different temperatures. Phase fraction evolution is obtained from *in-situ* high-temperature synchrotron radiation diffraction measurement using cobalt and lithium hydroxides as precursors[5].

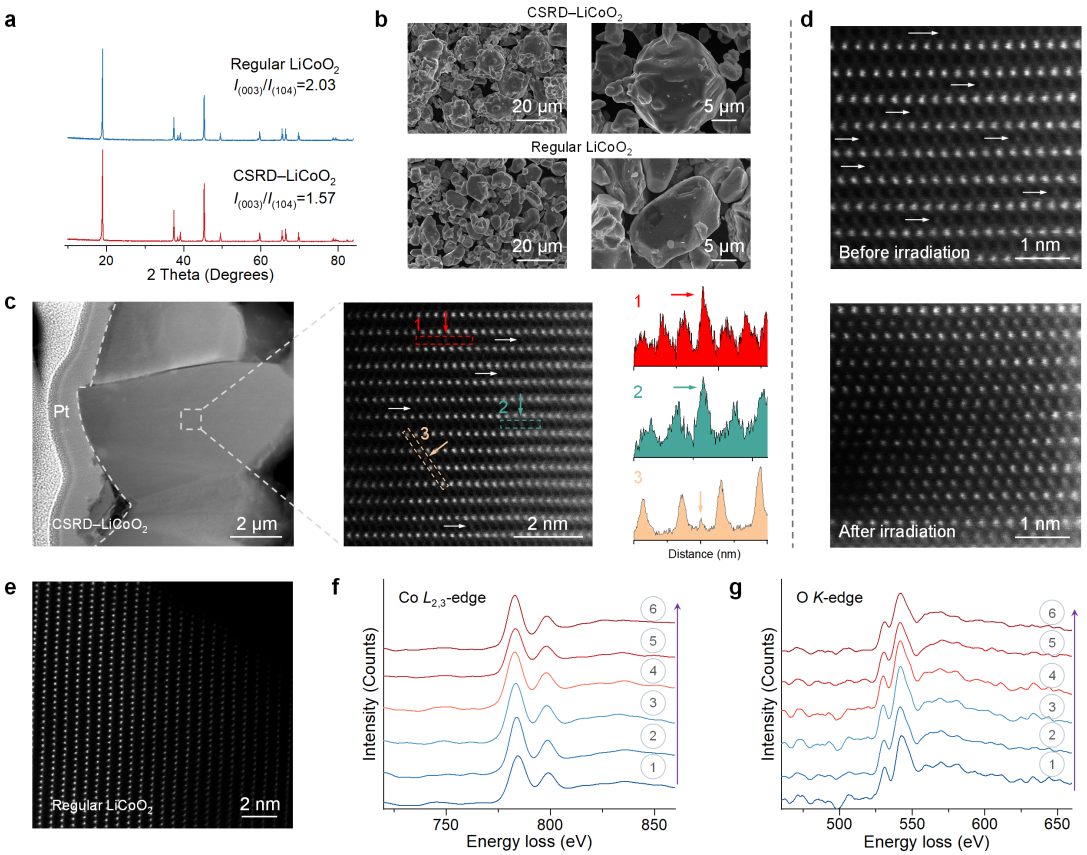

Supplementary Figure 16. Crystal structure of the regular $LiCoO_2$ and the CSRD–$LiCoO_2$ materials. a, XRD patterns from different synthesis methods. The blue pattern is obtained from the regular method and the red one is prepared by the improved method (See methods). **b**, SEM images of the CSRD−$LiCoO_2$ (top) and regular $LiCoO_2$ (bottom). **c**, SEM and TEM images of particle milled by focused ion beam (FIB) of the CSRD−$LiCoO_2$ material. Atomic-resolution STEM−HAADF image and line profiles along the different directions, where the arrows denote the local disorder distribution. **d**, STEM−HAADF images of the CSRD−$LiCoO_2$ material before and after long-time beam irradiation. To exclude the influence of beam irradiation, a control experiment was conducted, where after subjecting the sample for a longer time, more disorder appeared, which resulted in a distinct contrast from the as-prepared material. **e**, STEM−HAADF images of the regular $LiCoO_2$ material. **f**, STEM−EELS of Co *K*-edge in the CSRD−$LiCoO_2$ material. **g**, STEM−EELS of O *K*-edge in the CSRD−$LiCoO_2$ material. The corresponding line is shown in Fig. 2a.

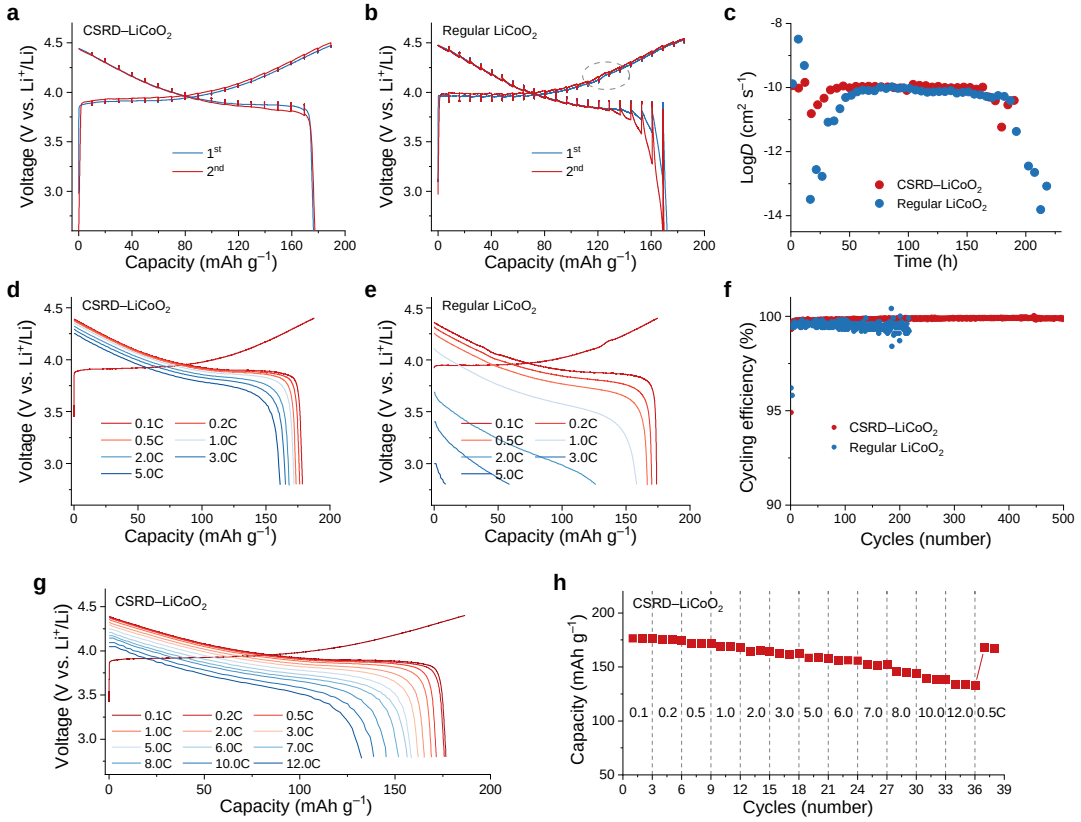

Supplementary Figure 17. Electrochemical performance. a,b, GITT curves of **(a)** the CSRD−$LiCoO_2$ cathode and **(b)** the regular $LiCoO_2$ cathode for the first two cycles. **c**, Li-ion diffusivity vs. cycling time for the different $LiCoO_2$ cathodes based on the first cycle in GITT measurement. **d**,**e**, Galvanostatic charge/discharge curves cycled between 2.8−4.4 V of **(d)** the CSRD−$LiCoO_2$ cathode and **(e)** the regular $LiCoO_2$ cathode at different rates. **f**, CEs in $LiCoO_2$||Li cells cycled between 2.8−4.4 V. **g**, Galvanostatic charge/discharge curves and **h**, capacity retention of the extended electrochemical rate test of the CSRD−$LiCoO_2$ cathode in 2.8−4.4 V.

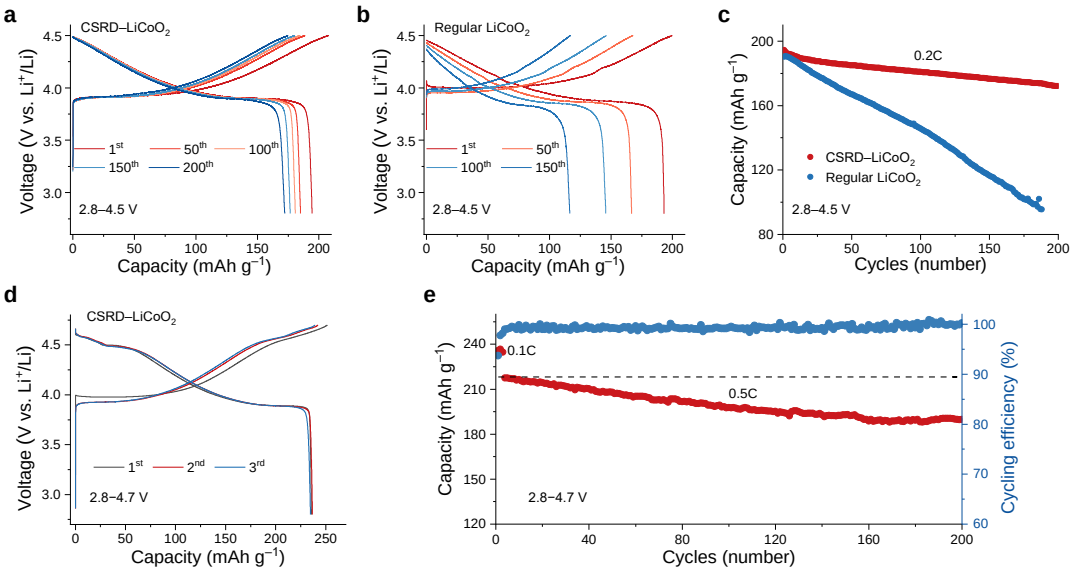

Supplementary Figure 18. Electrochemical performance at increased voltages. a,**b**, Galvanostatic charge/discharge curves of **(a)** the CSRD−$LiCoO_2$ cathode and **(b)** the regular $LiCoO_2$ cathode cycled between 2.8−4.5 V. **c**, Capacity retentions of the CSRD−$LiCoO_2$ cathode and regular $LiCoO_2$ cathode cycled between 2.8−4.5 V with an areal capacity of ~1.0 mAh cm^{-2}. **d**, Galvanostatic charge/discharge curves and **e**, capacity retention of the CSRD−$LiCoO_2$ cathode cycled between 2.8−4.7 V.

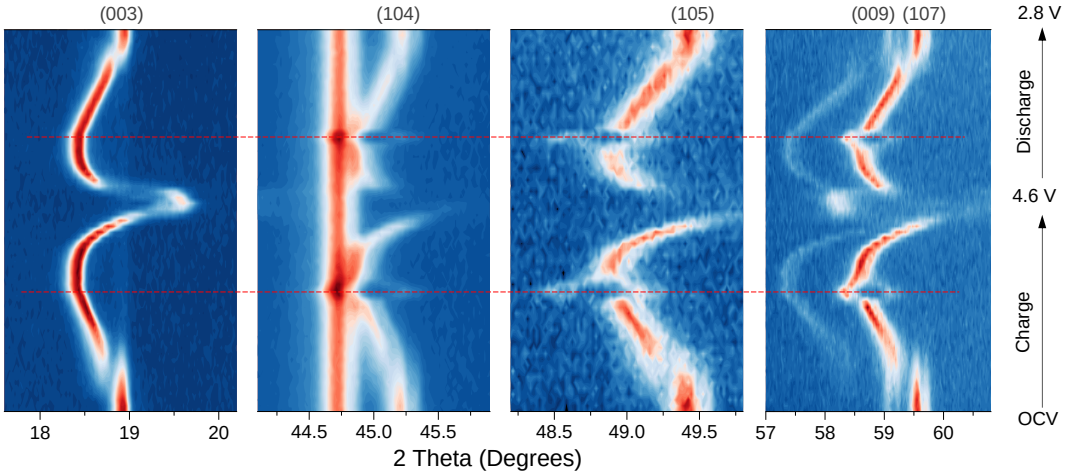

Supplementary Figure 19. *In-situ* XRD patterns of the regular $LiCoO_2$ cathode recorded at a current rate of 0.08C in the voltage range of 2.8−4.6 V. The red dash lines show the splitting of the (104), (105) and (107) reflections during cycling.

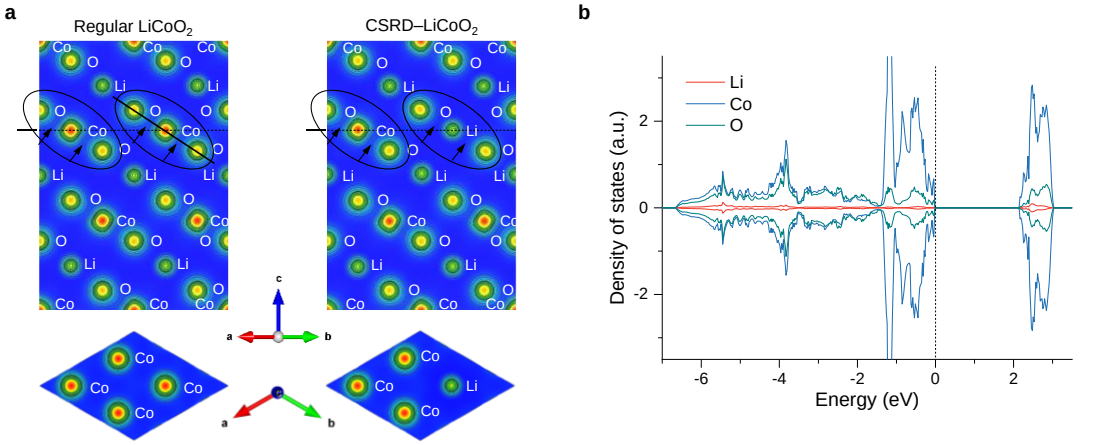

Supplementary Figure 20. Electronic structure information of $LiCoO_2$ materials. a, Charge density distribution of the pristine CSRD−$LiCoO_2$ material and regular $LiCoO_2$ material at $Li_{1.0}CoO_2$ composition. The red contour stands for high charge density while the blue is for low charge density. **b**, PDOS of the regular $LiCoO_2$ material. The dashed line represents the Fermi level at 0 eV.

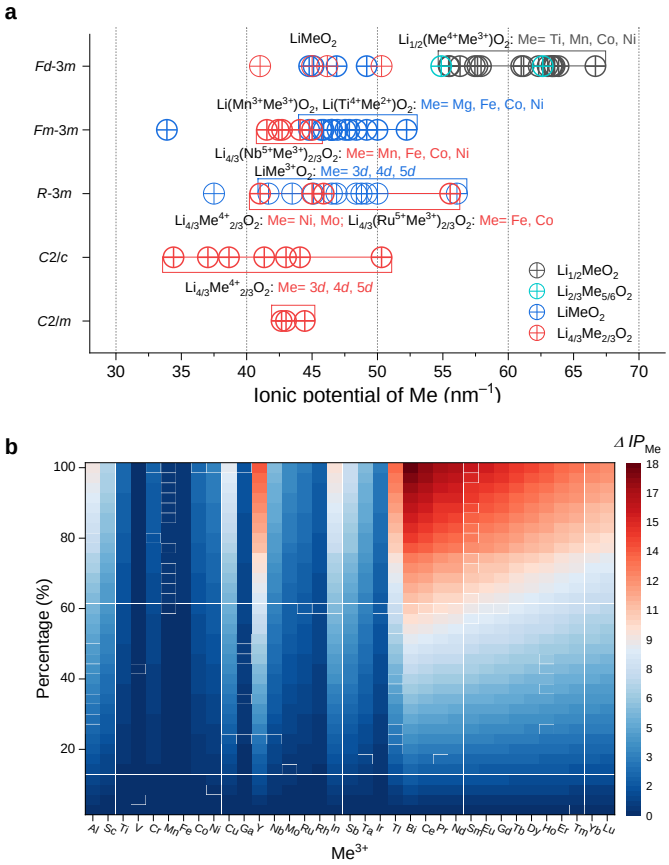

Supplementary Figure 21. Extension of the CSRD configuration to the $Li_xMe_yO_2$ system. a, Ionic potential of representative $Li_xMe_yO_2$, including $Li_{1/2}MeO_2$, $Li_{2/3}Me_{5/6}O_2$, $LiMeO_2$, and $Li_{4/3}Me_{2/3}O_2$ oxides with the Me in different compositions. **b**, The calculated ionic potential evolution between $Mg_{1/2}Ti_{1/2}$ and trivalent elements. The composition of $LiMg_{1/2}Ti_{1/2}O_2$ is selected as the starting model to generate the CSRD configuration in the $Li_xMe_yO_2$ system owing to its disordered crystal structure, relatively light atomic mass and charge compensation to Me^{3+} (Me^{3+}=1/2Mg^{2+}+1/2Ti^{4+}).

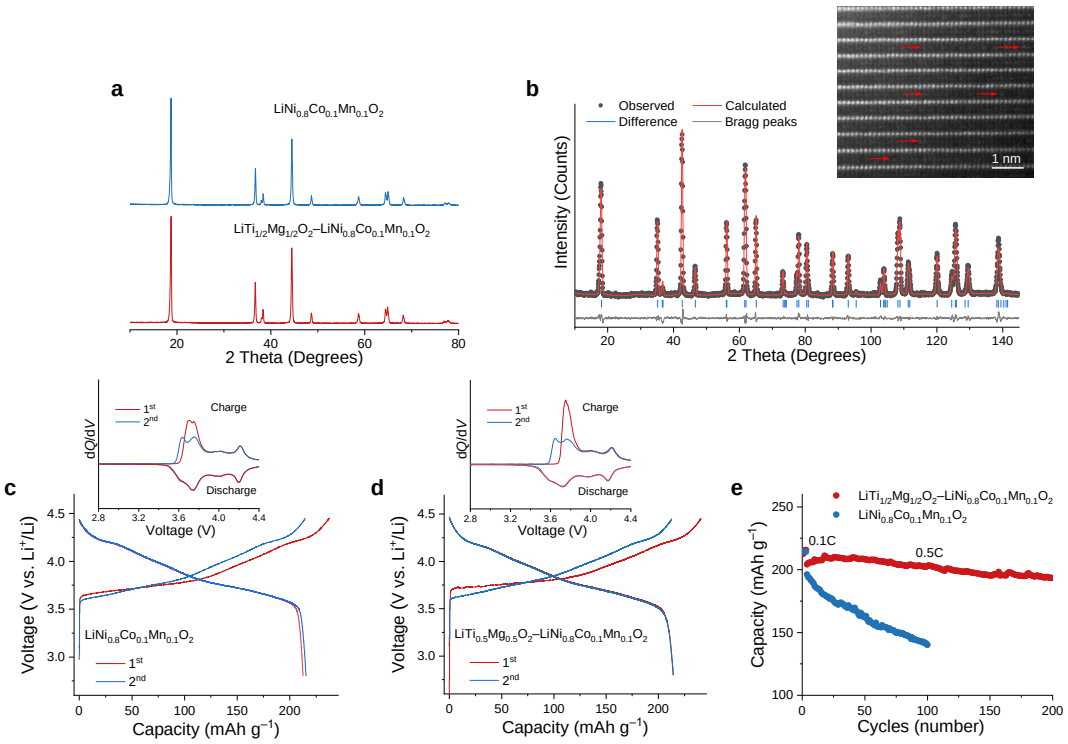

Supplementary Figure 22. Crystal structure and electrochemical performance of Ni-rich $LiNi_{0.8}Co_{0.1}Mn_{0.1}O_2$ materials with the CSRD configuration. a, XRD patterns of $LiNi_{0.8}Co_{0.1}Mn_{0.1}O_2$ materials. **b**, NPD pattern and STEM−HAADF image of the as-prepared $LiTi_{1/2}Mg_{1/2}O_2$−$LiNi_{0.8}Co_{0.1}Mn_{0.1}O_2$ material. **c**,**d**, Galvanostatic charge/discharge curves and the corresponding dQ/dV curves of **(c)** the $LiNi_{0.8}Co_{0.1}Mn_{0.1}O_2$ material and **(d)** the $LiTi_{1/2}Mg_{1/2}O_2$−$LiNi_{0.8}Co_{0.1}Mn_{0.1}O_2$ material. **e**, Cycling performance between 2.8−4.5 V under a 0.1C rate for the first three cycles before cycling at a 0.5C rate for both materials.

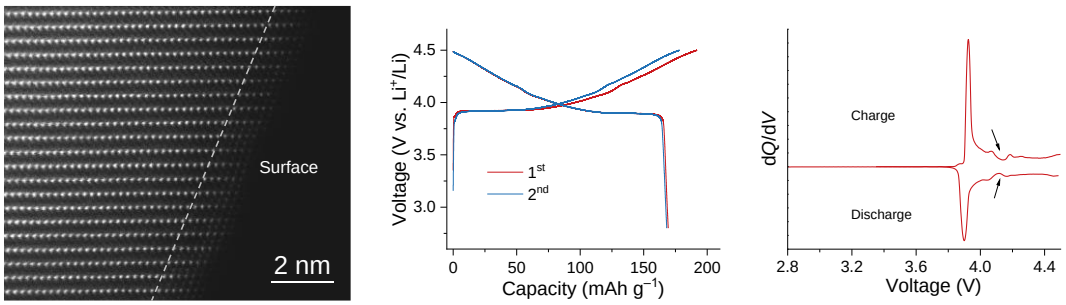

Supplementary Figure 23. STEM−HAADF image and cycling curves of the surface disordered $LiCoO_2$ material. A material with disordered atomic arrangements only exists in the surface of the particle has been obtained by mixing with $LiOH{\cdot}H_2O$ at a molar ratio of 1:1.03; then heated at 950 °C for 12 h, and then heated at 1,100 °C for 3 h, where the second heating aiming at offering a short time for the sample exposing in the higher temperature to induce the surface structure changes. The phase transition from Li^+/vacancy ordering appears for this $LiCoO_2$ cathode at around 4.15 V, corresponding to a hexagonal to monoclinic structure transition.

Supplementary Tables

Supplementary Table 1. Structural symmetry of $LiMeO_2$ compositions. Me is the trivalent ions.

	Fd-3*m* (227)	*Fm*-3*m* (225)	*R*-3*m* (166)	$I4_1/amd$ (141)	$I\text{-}4_2d$ (122)	$P4_12_12$ (92)	*Ibam* (72)	*Pbnm* (62)	*Pmnm* (59)	*Pnnm* (58)	$Pna2_1$ (33)	*C*2/*c* (15)	$P2_1/c$ (14)	*C*2/*m* (12)
$LiBO_2$					√								√	
$LiAlO_2$			√	√		√								
$LiScO_2$				√										
$LiTiO_2$	√	√						√						
$LiVO_2$	√		√											
$LiCrO_2$			√											
$LiMnO_2$		√		√					√					√
$LiFeO_2$		√	√	√	√						√	√		
$LiCoO_2$	√	√	√											
$LiNiO_2$		√	√											
$LiCuO_2$														√
$LiGaO_2$		√	√								√			
$LiYO_2$				√									√	
$LiNbO_2$			√											
$LiMoO_2$			√											√
$LiRuO_2$										√				
$LiRhO_2$	√		√											
$LiInO_2$			√	√										
$LiSbO_2$													√	
$LiTaO_2$														
$LiIrO_2$														
$LiTlO_2$		√		√						√				
$LiBiO_2$							√							
$LiCeO_2$													√	
$LiPrO_2$													√	
$LiNdO_2$													√	
$LiSmO_2$													√	
$LiEuO_2$													√	
$LiGdO_2$								√						
$LiTbO_2$								√					√	
$LiDyO_2$													√	
$LiHoO_2$													√	
$LiErO_2$				√									√	
$LiTmO_2$				√										
$LiYbO_2$				√										
$LiLuO_2$				√										

Supplementary Table 2. Ionic radius, oxidation state and ionic potential of Me^{3+} in $LiMeO_2$ compositions.

Oxide	Radii (Å)	Valence	$\overline{\Phi_{TM}}$ (nm^{-1})
$LiBO_2$	0.27	3	111.11111
$LiAlO_2$	0.535	3	56.074766
$LiScO_2$	0.745	3	40.268456
$LiTiO_2$	0.67	3	44.776119
$LiVO_2$	0.64	3	46.875
$LiCrO_2$	0.615	3	48.780488
$LiMnO_2$	0.645	3	46.511628
$LiFeO_2$	0.645	3	46.511628
$LiCoO_2$	0.61	3	49.180328
$LiNiO_2$	0.6	3	50
$LiCuO_2$	0.54	3	55.555556
$LiGaO_2$	0.62	3	48.387097
$LiYO_2$	0.9	3	33.333333
$LiNbO_2$	0.72	3	41.666667
$LiMoO_2$	0.69	3	43.478261
$LiRuO_2$	0.68	3	44.117647
$LiRhO_2$	0.665	3	45.112782
$LiInO_2$	0.8	3	37.5
$LiSbO_2$	0.76	3	39.473684
$LiTaO_2$	0.72	3	41.666667
$LiIrO_2$	0.68	3	44.117647
$LiTlO_2$	0.885	3	33.898305
$LiBiO_2$	1.03	3	29.126214
$LiCeO_2$	1.01	3	29.70297
$LiPrO_2$	0.99	3	30.30303
$LiNdO_2$	0.983	3	30.51882
$LiSmO_2$	0.958	3	31.31524
$LiEuO_2$	0.947	3	31.678986
$LiGdO_2$	0.938	3	31.982942
$LiTbO_2$	0.923	3	32.502709
$LiDyO_2$	0.912	3	32.894737
$LiHoO_2$	0.901	3	33.296337
$LiErO_2$	0.89	3	33.707865
$LiTmO_2$	0.88	3	34.090909
$LiYbO_2$	0.868	3	34.562212
$LiLuO_2$	0.861	3	34.843206

All Me^{3+} are calculated with high-spin ionic radius in six-coordination number.

Supplementary Table 3. Crystallographic and Rietveld refinement data of the as-prepared $LiCoO_2$ compound.

Space group	R-3m − Rhombohedral
Wavelengths	1.479728 Å
Temperature	~300 K
Cell parameters	$a = b$ = 2.818756(23) Å, c = 14.07166(20) Å $\alpha = \beta$ = 90°, γ = 120° V = 96.8260(20) Å^3, Z = 3
Reliability factors	R_{wp} = 7.37% R_p = 5.75% Gof = 2.09 R_F^2 = 1.99%

Supplementary Table 4. Atomic coordinates, occupancies and anisotropic displacement parameters (Å^2) of the as-prepared $LiCoO_2$ compound.

	x	y	z	Occupancy	U_{iso}	Wyckoff
Li1	0	0	0	0.97427(3)	0.00938(2)	3*b*
Co2	0	0	0	0.02573(1)	0.00938(2)	3*b*
Co3	0	0	1/2	0.97427(3)	0.0016(15)	3*a*
Li4	0	0	1/2	0.02573(1)	0.0016(15)	3*a*
O5	0	0	0.23951(5)	1.0	0.00399(33)	6*c*

Supplementary Table 5. Structural symmetry of representative $Li_xMe_yO_2$ oxides with the Me in different element compositions.

	Fd-3*m* (227)	*Fm*-3*m* (225)	*R*-3*m* (166)	*C*2/*c* (15)	*C*2/*m* (12)
$Li_{1/2}TiO_2$	√				
$Li_{1/2}VO_2$	√				√
$Li_{1/2}MnO_2$	√				
$Li_{1/2}CoO_2$	√				
$Li_{1/2}NiO_2$	√				
$Li_{2/3}Ti_{5/6}O_2$	√				
$Li_{2/3}Mn_{5/6}O_2$	√				
$Li_{4/3}Ti_{2/3}O_2$		√		√	
$Li_{4/3}Mn_{2/3}O_2$	√			√	
$Li_{4/3}Ni_{2/3}O_2$			√		
$Li_{4/3}Zr_{2/3}O_2$				√	
$Li_{4/3}Mo_{2/3}O_2$	√		√		
$Li_{4/3}Tc_{2/3}O_2$				√	
$Li_{4/3}Ru_{2/3}O_2$				√	√
$Li_{4/3}Rh_{2/3}O_2$					√
$Li_{4/3}Sn_{2/3}O_2$				√	
$Li_{4/3}Ir_{2/3}O_2$					√
$Li_{4/3}Pt_{2/3}O_2$					√
$Li_{4/3}Pb_{2/3}O_2$				√	
$LiTi_{1/2}Mg_{1/2}O_2$		√			
$LiTi_{1/2}V_{1/2}O_2$		√			
$LiTi_{1/2}Fe_{1/2}O_2$		√			
$LiTi_{1/2}Co_{1/2}O_2$		√			
$LiTi_{1/2}Ni_{1/2}O_2$		√			
$LiMn_{1/2}Ni_{1/2}O_2$		√			
$LiMn_{1/2}Fe_{1/2}O_2$		√			
$LiMn_{1/2}Co_{1/2}O_2$		√			
$Li_{1/2}Mn_{1/2}V_{1/2}O_2$	√				
$Li_{1/2}Ti_{1/2}Cr_{1/2}O_2$	√				
$Li_{1/2}Ti_{1/2}Mn_{1/2}O_2$	√				
$Li_{1/2}Ti_{1/2}Fe_{1/2}O_2$	√				
$Li_{1/2}Ti_{1/2}Co_{1/2}O_2$	√				
$Li_{1/2}Ru_{1/2}Fe_{1/2}O_2$	√				
$Li_{1/2}Mn_{3/4}Mg_{1/4}O_2$	√				
$Li_{1/2}Mn_{3/4}Fe_{1/4}O_2$	√				
$Li_{1/2}Mn_{3/4}Co_{1/4}O_2$	√				
$Li_{1/2}Mn_{3/4}Ni_{1/4}O_2$	√				
$Li_{1/2}Mn_{3/4}Cu_{1/4}O_2$	√				
$Li_{1/2}Mn_{3/4}Zn_{1/4}O_2$	√				

$Li_{4/3}Nb_{1/3}Mn_{1/3}O_2$		√	
$Li_{4/3}Nb_{1/3}Fe_{1/3}O_2$		√	
$Li_{4/3}Nb_{1/3}Co_{1/3}O_2$		√	
$Li_{4/3}Nb_{1/3}Ni_{1/3}O_2$		√	
$Li_{4/3}Ru_{1/3}Fe_{1/3}O_2$	√	√	√
$Li_{4/3}Ru_{1/3}Co_{1/3}O_2$			√
$Li_{4/3}Ru_{1/3}Ni_{1/3}O_2$	√		

Supplementary Table 6. Ionic radius, oxidation state and ionic potential of $Li_xMe_yO_2$ oxides.

	Radii Me1 (Å)	Radii Me2 (Å)	Valence Me1	Valence Me2	Φ_{Me1}	Φ_{Me2}	$\overline{\Phi_{Me}}$
$Li_{1/2}TiO_2$	0.67	0.605	3	4	44.77612	66.1157	55.44591
$Li_{1/2}VO_2$	0.64	0.58	3	4	46.875	68.96552	57.92026
$Li_{1/2}MnO_2$	0.645	0.53	3	4	46.51163	75.4717	60.99166
$Li_{1/2}CoO_2$	0.61	0.53	3	4	49.18033	75.4717	62.32601
$Li_{1/2}NiO_2$	0.6	0.48	3	4	50	83.33333	66.66667
$Li_{2/3}Ti_{5/6}O_2$	0.605			4	66.1157		54.87603
$Li_{2/3}Mn_{5/6}O_2$	0.53			4	75.4717		62.64151
$Li_{4/3}Ti_{2/3}O_2$	0.605			4	66.1157		44.07713
$Li_{4/3}Mn_{2/3}O_2$	0.53			4	75.4717		50.31447
$Li_{4/3}Ni_{2/3}O_2$	0.48			4	83.33333		55.55556
$Li_{4/3}Zr_{2/3}O_2$	0.72			4	55.55556		37.03704
$Li_{4/3}Mo_{2/3}O_2$	0.65			4	61.53846		41.02564
$Li_{4/3}Tc_{2/3}O_2$	0.645			4	62.0155		41.34367
$Li_{4/3}Ru_{2/3}O_2$	0.62			4	64.51613		43.01075
$Li_{4/3}Rh_{2/3}O_2$	0.6			4	66.66667		44.44444
$Li_{4/3}Sn_{2/3}O_2$	0.69			4	57.97101		38.64734
$Li_{4/3}Ir_{2/3}O_2$	0.625			4	64		42.66667
$Li_{4/3}Pt_{2/3}O_2$	0.625			4	64		42.66667
$Li_{4/3}Pb_{2/3}O_2$	0.775			4	51.6129		34.4086
$LiTi_{1/2}Mg_{1/2}O_2$	0.72	0.605	2	4	27.77778	66.1157	46.94674
$LiTi_{1/2}V_{1/2}O_2$	0.79	0.605	2	4	25.31646	66.1157	45.71608
$LiTi_{1/2}Fe_{1/2}O_2$	0.78	0.605	2	4	25.64103	66.1157	45.87836
$LiTi_{1/2}Co_{1/2}O_2$	0.745	0.605	2	4	26.84564	66.1157	46.48067
$LiTi_{1/2}Ni_{1/2}O_2$	0.69	0.605	2	4	28.98551	66.1157	47.5506
$LiMn_{1/2}Ni_{1/2}O_2$	0.69	0.53	2	4	28.98551	75.4717	52.2286
$LiMn_{1/2}Fe_{1/2}O_2$	0.645	0.645	3	3	46.51163	46.51163	46.51163
$LiMn_{1/2}Co_{1/2}O_2$	0.645	0.61	3	3	46.51163	49.18033	47.84598
$Li_{1/2}Mn_{1/2}V_{1/2}O_2$	0.64	0.53	3	4	46.875	75.4717	61.17335
$Li_{1/2}Ti_{1/2}Cr_{1/2}O_2$	0.615	0.605	3	4	48.78049	66.1157	57.4481
$Li_{1/2}Ti_{1/2}Mn_{1/2}O_2$	0.645	0.605	3	4	46.51163	66.1157	56.31367
$Li_{1/2}Ti_{1/2}Fe_{1/2}O_2$	0.645	0.605	3	4	46.51163	66.1157	56.31367
$Li_{1/2}Ti_{1/2}Co_{1/2}O_2$	0.61	0.605	3	4	49.18033	66.1157	57.64802
$Li_{1/2}Ru_{1/2}Fe_{1/2}O_2$	0.645	0.62	3	4	46.51163	64.51613	55.51388
$Li_{1/2}Mn_{3/4}Mg_{1/4}O_2$	0.72	0.53	2	4	27.77778	75.47170	63.54822
$Li_{1/2}Mn_{3/4}Fe_{1/4}O_2$	0.78	0.53	2	4	25.64103	75.47170	63.01403
$Li_{1/2}Mn_{3/4}Co_{1/4}O_2$	0.745	0.53	2	4	26.84564	75.47170	63.31518
$Li_{1/2}Mn_{3/4}Ni_{1/4}O_2$	0.69	0.53	2	4	28.98551	75.47170	63.85015
$Li_{1/2}Mn_{3/4}Cu_{1/4}O_2$	0.73	0.53	2	4	27.39726	75.47170	63.45309
$Li_{1/2}Mn_{3/4}Zn_{1/4}O_2$	0.74	0.53	2	4	27.02703	75.47170	63.36053
$Li_{4/3}Nb_{1/3}Mn_{1/3}O_2$	0.645	0.64	3	5	46.51163	78.125	41.54554

$Li_{4/3}Nb_{1/3}Fe_{1/3}O_2$	0.645	0.64	3	5	46.51163	78.125	41.54554
$Li_{4/3}Nb_{1/3}Co_{1/3}O_2$	0.61	0.64	3	5	49.18033	78.125	42.43511
$Li_{4/3}Nb_{1/3}Ni_{1/3}O_2$	0.6	0.64	3	5	50	78.125	42.70833
$Li_{4/3}Ru_{1/3}Fe_{1/3}O_2$	0.645	0.565	3	5	46.51163	88.49558	45.0024
$Li_{4/3}Ru_{1/3}Co_{1/3}O_2$	0.61	0.565	3	5	49.18033	88.49558	45.89197
$Li_{4/3}Ru_{1/3}Ni_{1/3}O_2$	0.6	0.565	3	5	50	88.49558	46.16519

Supplementary Table 7. Crystallographic and Rietveld refinement data of the as-prepared $LiTi_{1/2}Mg_{1/2}O_2$–$LiNi_{0.8}Co_{0.1}Mn_{0.1}O_2$ compound.

Space group	*R*-3*m* − Rhombohedral
Wavelengths	1.479728 Å
Temperature	~300 K
Cell parameters	$a = b$ = 2.88084(5) Å, c = 14.21427(33) Å $\alpha = \beta$ = 90°, γ = 120° V = 102.163(4) Å^3, Z = 3
Reliability factors	R_{wp} = 6.33% R_p = 4.75% *Gof* = 1.54 R_F^2 = 5.83%

Supplementary Table 8. Atomic coordinates, occupancies and anisotropic displacement parameters (Å^2) of the as-prepared $LiTi_{1/2}Mg_{1/2}O_2$–$LiNi_{0.8}Co_{0.1}Mn_{0.1}O_2$ compound.

	x	y	z	Occupancy	U_{iso}	Wyckoff
Li1	0	0	1/2	0.95887(2)	0.0637(3)	3*b*
Mg2	0	0	1/2	0.00635(2)	0.0637(3)	3*b*
Ti3	0	0	1/2	0.00557(2)	0.0637(3)	3*b*
Ni4	0	0	1/2	0.02921(2)	0.0637(3)	3*b*
Ni5	0	0	0	0.7545(1)	0.0042(2)	3*a*
Co6	0	0	0	0.09821(1)	0.0042(2)	3*a*
Mn7	0	0	0	0.1028(1)	0.0042(2)	3*a*
Mg8	0	0	0	0.00365(1)	0.0042(2)	3*a*
Ti9	0	0	0	0.00443(1)	0.0042(2)	3*a*
Li10	0	0	0	0.03641(1)	0.0042(2)	3*a*
O11	0	0	0.25815(15)	0.9922(16)	0.0222(2)	6*c*

References

1 Zhao, C., Avdeev, M., Chen, L. & Hu, Y.-S. An O3-type Oxide with Low Sodium Content as the Phase-Transition-Free Anode for Sodium-Ion Batteries. *Angewandte Chemie International Edition* **57**, 7056-7060 (2018).

2 Shannon, R. D. Revised effective ionic radii and systematic studies of interatomic distances in halides and chalcogenides. *Acta Crystallographica Section A* **32**, 751-767 (1976).

3 Kim, J. *et al.* Prospect and Reality of Ni-Rich Cathode for Commercialization. *Advanced Energy Materials* **8**, 1702028 (2018).

4 Lu, Z., MacNeil, D. D. & Dahn, J. R. Layered $LiNi_xCo_{1-2x}Mn_xO_2$ Cathode Materials for Lithium-Ion Batteries. *Electrochemical and Solid-State Letters* **4**, A200 (2001).

5 Hua, W. *et al.* Chemical and Structural Evolution during the Synthesis of Layered $Li(Ni,Co,Mn)O_2$ Oxides. *Chemistry of Materials* **32**, 4984-4997 (2020).